Biotemplated Zinc Sulfide Nanofibers as Anode Materials for Sodium-Ion Batteries

Citation: Zhang, Geran et al. "Biotemplated Zinc Sulfide Nanofibers as Anode Materials for Sodium-Ion Batteries." ACS Applied Nano Materials 1, 10 (September 2018): 5631–5639 © 2018 American Chemical Society

As Published: http://dx.doi.org/10.1021/acsanm.8b01254

Publisher: American Chemical Society (ACS)

Persistent URL: https://hdl.handle.net/1721.1/126086

Version: Author's final manuscript: final author's manuscript post peer review, without publisher's formatting or copy editing

Biotemplated zinc sulfide nanofibers as anode materials for sodium-ion batteries

*Geran Zhang†‡@, Shuya Wei†‡§@, and Angela M. Belcher†‡§**

†Department of Materials Science and Engineering, Massachusetts Institute of Technology, Cambridge, Massachusetts 02139, United States

‡ The Koch Institute for Integrative Cancer Research, Massachusetts Institute of Technology, Cambridge, Massachusetts 02139, United States

§ Department of Biological Engineering, Massachusetts Institute of Technology, Cambridge, Massachusetts 02139, United States

@ These authors contributed equally.

Formatted: TA_Main_Text

Formatted: Font: Times

KEYWORDS

Zinc sulfide, nanofiber, biotemplating, sodium-ion battery, electrochemistry

ABSTRACT

Sodium-ion batteries have generated substantial interest due to the g~~G~~eopolitical uncertainties in the access to lithium as well as ~~in access to lithium combined with~~with the potential cost savings associated with replacing lithium with sodium~~ have generated renewed interest in sodium-ion batteries~~. One of the key technological impediments to sodium-ion batteries is the availability of a low cost, high capacity anode material. Here, we show that biotemplated zinc sulfide nanofibers, prepared using the M13 bacteriophage template, ~~have good potential to be used for this purpose~~have significant potential to be used for this purpose. We investigated the effect of both annealing and molecular templated carbon-coating on the electrochemical performance of these materials. Biotemplated zinc sulfide nanofibers, when coated with a ~~~~<~~2 nm carbon layer, could deliver a reversible capacity of 603 mAh/g at 100 mA/g discharge rate, even ~~with a high overall zinc sulfide loading of~~when the zinc sulfide loading is as high as 70%. Initial Coulombic efficiency was ~~as high as~~reached 71%, and the ~~cell~~ anode could be cycled for at least 100 cycles.

TEXT

Introduction

Biotemplating is a technique ~~which is based on using~~ which uses biological structures to direct the growth of materials, usually under mild and aqueous conditions~~. Biological structures have been used as biological templates to make many types of materials~~[1,2]. The M13 bacteriophage has been shown to be a particularly versatile biotemplate due to its genetic tunability and safety[3–6]. The M13 bacteriophage is a filamentous virus with diameter ~6.5 nm and length ~880 nm, and has

already been used to make many 1-~~one~~-dimensional materials of technological importance for applications ranging from energy storage and conversion to~~, energy conversion and~~ heterogeneous catalysis[7–9]. Zinc sulfide is a II-VI group semiconducting compound with main applications in photocatalysis, pigments, photoluminescent screens and optoelectronics[10–13]. Here, we use the M13 bacteriophage to prepare zinc sulfide nanofibers as anode materials in sodium-ion batteries (SIBs)[14,15].

There has been a resurgence in interest in SIBs due to concerns over the geopolitical availability of lithium as well as ~~nd~~ potential cost savings derived from moving away from lithium[16–19]. SIBs were first realized as far back as 1980, when the reversible intercalation of sodium into titanium disulfide was demonstrated. However, research on SIBs decrease in favor of lithium-ion batteries (LIBs). One challenge is that the sodium ion is larger than lithium (mass: 23 amu vs. 6.94 amu, ionic radius: 1.02 Å vs. 0.76 Å), which means it is harder to develop materials that enable topologically stable intercalation of the sodium ion[20,21]. This is much less problematic on the cathode side, where layered oxides of the form Na_xMO_2 (M = Fe, Mn, Co, Ni, Cr, V) have been demonstrated to be potential candidates as intercalation-type cathodes[22,23]. The major obstacle proved to be the absence of a suitable anode material. Like its lithium analogue, ~~sodium metal is hard to be directly used as an anode material~~it is difficult to use pure sodium metal as an anode material. This is because the repetitive deposition and stripping of these alkali metals during charge and discharge cycles causes significant morphological changes to the metal surface (for example, dendrite formation) and loss of material density. Continuous change in morphology means the continued formation ~~of a solid-electrolyte and~~ and breaking of a solid-electrolyte interphase (SEI), resulting in poor Coulombic efficiency and quasi-reversibility[24,25]. In the case of LIBs, graphite

~~acts~~ can act as an intercalation host for lithium ions at ~~, with a reduction potential of~~ 0.1~0.2 V ~~and~~ to a capacity of 372 mAh/g, ~~and is therefore an~~making it an ideal anode material. Unfortunately, sodium ions cannot intercalate into graphite, which means this important anode material cannot be used in SIBs. Currently, the most studied anode material for SIBs is hard carbon which has a reversible capacity of ~300 mAh/g below 0.5 V[26]. In the continued search for high capacity anode materials, conversion type oxides and sulfides have ~~another class of materials emerged that is particularly interesting – metal sulfides~~ emerged as classes of materials that~~, which~~ promise~~s~~ significantly higher capacity than hard carbons. Metal sulfides are particularly interesting because, compared to oxides, they exhibit higher electrical conductivity, richer redox chemistry, and ~~,~~ enhanced redox kinetics due to the lower binding energy~~and benefits from a weak metal-sulfide bond that make reactions kinetically favourable~~[21,27,28].

~~Most~~So far, most of the work on metal sulfides has been on layered sulfides such as MoS_2, WS_2 and SnS_2[29,30]. While many of these materials ~~have shown very~~ demonstrate good electrochemical properties, ~~but due to the high prices of some of these metals~~the high raw material costs of these metals may limit their practical application (Table 1) ~~(Table 1), it makes sense to explore other types of metal sulfides~~. Zinc sulfide is interesting because of its low cost and high abundance. Its reaction with sodium is mostly conversion-based, although zinc metal does exhibit some alloying with sodium. The total theoretical capacity is 571 mAh/g, and the overall electrochemical process is given below. ~~In fact, interest in SIBs largely stems from potential cost savings compared to LIBs. In general, 70~80% of the total cost of a battery cell can be attributed to material costs[30,31]. Of this, 40~50% is attributed to active materials and ~15% to the current collectors. With SIBs, we not only save on the cost and the geopolitical uncertainty of lithium (lithium carbonate is priced~~

~~at $7400 per ton) compared to sodium (soda ash is priced at $143 per ton), but it also allows aluminum ($0.8 per lb.) to be used as the anode side current collector as opposed to copper ($2.20 per lb.)[32]. This is not possible in LIBs because lithium alloys with aluminum at low potentials.~~

~~The cost and abundance let us investigate the low cost biotemplated zinc sulfide as a anode material. On the basis of two type of reactions with sodium: a conversion reaction first to form sodium sulfide and metallic zinc, followed by an alloying reaction of sodium ions with zinc, zinc sulfide promised a theoretical capacity of 571 mAh/g.~~

$$ZnS + 2Na^+ + 2e^- \rightarrow Na_2S + Zn$$

$$13Zn + Na^+ + e^- \rightarrow NaZn_{13}$$

Diffusion kinetics in these sulfide anode materials can be improved using nanostructured materials and controlling the nanoscale dimensions[21]. In addition, nanostructured composites of sulfide nanoparticles with carbon were shown to improve conductivity and pseudocapacitance, therefore enhancing reversible capacity and rate capability[31]. In this work, we prepared zinc sulfide nanofibers using a process called biotemplating. We further investigated the effects of annealing and carbon-coating on these nanofibers for enhancing electrochemical activity.

Results and Discussion

Material synthesis and characterization

Zinc sulfide (sphalerite) nanofibers were synthesized using the M13 bacteriophage as a physical template to direct particle precipitation and local aggregation. The as-prepared nanofibers were then coated modified with very thin layer of carbon-coating (<2 nm) using a phenolic resin precursor. The overall synthesis process is schematically illustrated in Figure 1. In the zinc sulfide synthesis, zinc acetate was used as the zinc precursor –although other zinc salts such as zinc nitrate were equally effective. Thioacetamide was used as the *in situ* sulfur source. The overall reaction is given by Equation 1.

$$Zn^{2+} + CH_3C(S)NH_2 + H_2O \rightarrow ZnS + CH_3C(O)NH_2 + 2H^+ \quad (1)$$

This reaction is relatively general and is widely employed in the synthesis of sulfides of transition metals (M = Zn, Cu, Ni, Pb, Hg, Cd, Sn)[32–34]. Nanofiber formation follows a precipitation-aggregation type mechanism. In the first stage of the reaction, primary zinc particles of size 5~10 nm formed. These particles nucleated quickly onto the surface of the virus template, possibly by a combination of van der Waals interactions and specific interaction with the functional moieties on the virus coat protein. The appearance of sometimes hollow interiors, particularly if thioacetamide was added into a preheated solution before zinc acetate, suggesteds that this was a rapid aggregation process.

Zinc sulfide nanofibers were synthesized by carrying out the reaction in the presence of the M13 bacteriophage, which acted as a physical template onto which zinc sulfide nanoparticles could nucleate. Wild-type and genetically modified M13 bacteriophage were compared as the virus template. The M13 bacteriophage was genetically modified by inserting a four amino acid motif

(EEAE) into the p8 coat protein[4]. This motif was chosen because carboxylic acids are known to interact strongly with transition metal~~s~~ ions through chelation and electrostatic interaction (at above pH ~5). This modification gave the M13 bacteriophage particularly strong affinity for the zinc ion. Zinc sulfide nanofibers synthesized using the EEAE clone are shown in Figure 2. By comparison, when wild-type M13 bacteriophage was used as the template, a large number of spherical, non-templated particles were formed instead of nanofibers (Figure S1). However, because of this strong protein-ion interaction and the fact that zinc is a divalent ion with substantial charge screening, bundling of the virus was observed as soon as the zinc precursor was added into the~~a~~ virus ~~solution~~suspension. To minimize ~~this~~bundling, three strategies were used: (1) ~~minimizing precursor concentrations~~precursor concentration was minimized, (2) ~~hot injecting reactants~~reactants were introduced into a preheated solution by hot-injection and (3) ~~eliminating mechanical agitation~~no mechanical agitation was applied. Hot injection is a common strategy used in the solvothermal synthesis of nanoparticles using organometallic precursors. By injecting a cold precursor into a higher temperature reaction solution, the local temperature of the solution ~~was~~ could be temporarily reduced, ~~ therefore allowing~~which therefore allowed ~~–~~ nucleation to be controlled~~the number of nuclei formed to be controlled~~. As the local temperature of the reaction solution returned to its initial value, ~~subsequent~~ growth of the nuclei occurred in lieu of further nucleation ~~(nucleation occurs in at a lower temperature range compared to grow~~since this typically occurs at a higher temperature than nucleation~~th)~~[35]. In synthesizing zinc sulfide nanofibers, it was thought that hot injection allowed ~~the~~ immediate nucleation ~~of nuclei~~ onto the viral capsid. The immediate formation of negatively-stabilized zinc sulfide nuclei averted zinc ion-induced virus bundling. Also, somewhat counterintuitively, the absence of mechanical agitation ~~(stirring/shaking)~~such as stirring or shaking ~~–~~significantly improved nanofiber morphology. In

general, mechanical agitation ~~ensured~~ ensures uniform precursor depletion by convective ion transport~~ to facilitate uniform particle precipitation~~. However, because the virus template was particularly susceptible to zinc ion-induced bundling, convective motion ~~increased the~~was thought to increase the probability of ~~a~~ virus-to-virus collisions~~, each of~~ which ~~had some chance of forming~~led to q~~ a q~~uasi-irreversible contact ~~eventually leading to the~~and the formation of ~~a~~ virus bundles. ~~In the absence of agitation, viruses were limited to Brownian motion with a lower probability for collision.~~

While the reaction ~~seemed~~ was relatively insensitive to the zinc precursor, using thioacetamide as the sulfur source was particularly important. In preliminary experiments, sulfide anions (sodium sulfide or potassium sulfide) were used directly to precipitate various metal sulfides. In these cases, precipitation occurred almost instantaneously when the sulfide source was added. This rapid precipitation prohibited any control over nucleation and growth kinetics, and afforded no control over particle morphology, ~~,~~ even when the reaction was carried out at a low temperature (4 °C). On the other hand, nucleation kinetics could be controlled with thioacetamide by tuning temperature and precursor concentration. Under the precursor concentrations used (5 mM zinc acetate and 15 mM thioacetamide), no reaction was found to occur below 80 °C. Thioacetamide was used in 3-fold ~~ time~~ molar excess, because for ~~any~~ aqueous reaction involving transition metals there is ~~always~~ generally a competing precipitation of the transition metal by hydroxide anions in solution, which is particularly important under higher pH[36]. The reaction temperature was limited by the boiling point of water to 100 °C. In order to facilitate large liter-scale reactions, a temperature of 95 °C was used to avoid the need for reflux.

To improve electrochemical performance, the as-prepared zinc sulfide nanofibers were either modified with post annealing at 600 °C (sample M13-ZnS600), or modified with a thin carbon ~~n~~ coating ~~(1~2 nm)~~. Carbon, particularly hard carbon, is able to store sodium ions and has been shown to improve the performance of sulfide anodes[37]. ~~The latter was done by coating~~Carbon-coating was prepared by first coating the ~~material~~ zinc sulfide nanofibers ~~was~~ with a layer of phenolic resin, which was then carbonized in Argon~~followed by carbonization~~. A maximum carbonization temperature of 600 °C was used to ~~avoid~~ avoid thermal decomposition of zinc sulfide at higher temperatures.

The morphology of the nanofibers was ~~viewed~~ examined using TEM. Each nanofiber was 500~1000 nm in length, around the same length as a single M13 bacteriophage (Figure 2), which suggested that each nanofiber contained only a single virus template. This confirmed that virus bundling had been significantly minimized or eliminated since virus bundling would have resulted in nanofibers that were significantly longer. ~~The~~ A single virus core could be resolved in some nanofibers. Most nanofibers showed a hollow interior, which agreed with a precipitation-aggregation mechanism for nanofiber formation. The lattice fringes from high-resolution TEM micrographs (3.1 Å corresponding to the {111} planes~~, ICDD 04-016-4810~~) and ED pattern ~~pattern~~ confirm a β-ZnS crystal structure (ICDD 04-016-4810). The mass percentage of the organic residue~~s in each sample,~~ attributed to the virus template as well as the ~~and~~ carbon ~~-~~coating were~~,~~ ~~was~~ measured using TGA (Figure 3f). Four distinct regions of weight loss were observed. Region 1 (< 200 °C) was only observed in as-prepared nanofibers (M1~~E~~3-ZnS) and was attributed to the loss of adsorbed water. Region 2 (~345 °C) was also only observed in M1~~E~~3-ZnS and was attributed to the oxidative decomposition of the virus template. Region 3 (~550 °C) was only

observed in the carbon-coated sample (M13-ZnS600C) ~~C600~~, and was attributed to the combustion of the carbon ~~-~~coating. Region 4 (640~660 °C) was observed in all three samples, and was attributed to the oxidation of zinc sulfide to zinc oxide. Assuming complete oxidation, the initial weight percentage of zinc sulfide could be estimated by factoring in the molar mass ratio of zinc sulfide-to-zinc oxide. Based on this, we estimated that ~~which meant~~ the M13 bacteriophage took up ~10% of the mass of the as-prepared nanofiber. ~~the final nanofiber mass.~~ The annealed sample (M13-ZnS600) was almost entirely zinc sulfide (within the experimental error for TGA of ±1 wt. %), which was commensurate with the absence of peaks associated with the decomposition of organic and carbon species. ~~Zinc sulfide weight percentages are tabulated in Table 2.~~ This ~~meant~~ also implied that in the annealing process, all of the virus was decomposed. To ~~check~~ confirm this, we conducted TGA on pure virus and showed that at least 70~80 % of the mass of the virus was lost by annealing in nitrogen up to 600 °C. Zinc sulfide weight percentages are tabulated in Table 2.

Phase purity of the sulfide nanofibers was confirmed using a combination of XRD and XPS. The XRD for all samples showed four major peaks at 28.9°, 48.1°, 57.1° and 77.8° ~~were observed in their diffractograms~~ corresponding to the (111), (220), (311) and (331) diffraction planes of cubic phase sphalerite ~~((Figure 3e). The diffraction pattern was matched against reference card~~ ICDD 04-016-4810) ~~(ZnS, cubic F-43m, a = 5.34 Å)~~. Following annealing or carbonization, a smaller peak at ~28° emerged, although this peak may also have been present in the as-prepared as suggested by the asymmetry of the 28.9° peak. This small peak as well as another minute peak at ~37° were attributed to hexagonal phase wurtzite (JCPDS 75-1534). This cubic-to-hexagonal phase transition during thermal annealing was in agreement with previous reports [38]. The

proportion of this hexagonal phase was small, and was not believed to influence subsequent electrochemical tests significantly. ~~A small amount of contaminant phase was observed by XRD by two small peaks at ~28° and ~36° 2θ, although the phase could not be identified.~~ Primary particle size was estimated from the full width at half maximum (FWHM) of the 48.1° peak using the Scherrer equation, accounting for both microstrain and Caligioti contributions. By this measure, the primary particle size for the as-prepared nanofibers was 4.4 nm, while after annealing and ~~/~~carbon-coating, the particle size increased to 9.6 and ~~/~~9.5 nm, respectively. This increase in primary particle size was also ~~easily~~ clearly visible under TEM (Figure 3a-c). The increase in particle size was also reflected in the decrease in surface area from 26.1 m^2/g to 18.9 m^2/g after annealing. The higher surface area of 74.2 m^2/g for the carbon-coated sample was mainly attributed to the microporous carbon~~-~~ coating. The physical properties and composition of the different biotemplated zinc sulfide nanofibers are summarized in Table 2. XPS gave complementary information about the ionic valence and bonding states of zinc (Figure S2). The $Zn2p_{1/2}$ peak for the as-prepared and annealed samples was 1022.1 eV, corresponding to pure zinc sulfide. With carbon-coating, this peak shifted slightly to 1021.8 eV, ~~which suggested~~suggesting a minute ~~about~~ amount of zinc reduction during carbonization, and therefore a slight drop in Zn^{2+} valence state. A thin layer of carbon coating ~~<2 nm~~ was confirmed using TEM (Figure 3d). This carbon coating in general was ~2 nm, although thickness was slightly variable.

Electrochemical performance

Biotemplated zinc sulfide nanofibers were tested as anode materials for SIBs ~~using~~ in CR2032 coin cells ~~against a~~using a pure sodium metal counter electrode. In order to get the best practical

indication of electrochemical performance, the working electrode was prepared by mixing zinc sulfide nanofibers with Super P and PVDF in the academic standard ratio of 8:1:1. The gravimetric capacity was normalized against total nanofiber mass to account for dilution of active zinc sulfide mass due to the presence of organic (virus and carbon) components. Areal loading of the electrodes was ~1.1 mg/cm^2 and average thickness was ~30 μm. Volumetric capacities were calculated using the averaged areal loading and thickness.

We ran initial galvanostatic cycles at 50 mA/g between 0 and 3 V to compare the effect of annealing and carbon-coating on accessible capacity (Figure 4a-b). As with most ~~nano-sized~~nanoscale anode materials with a reduction potential lower than 1~1.5 V, the first discharge carried a large non-reversible component due to the formation of the SEI. ~~The important responses were the first cycle Coulombic efficiency (CE), the average discharge voltage and the reversible capacity~~ therefore t~~.~~he ~~The~~ reversible capacity was taken to be the second discharge capacity. ~~Reversible capacity increased with annealing and increased further with carbon coating.~~ Annealing increased the reversible capacity from 252 mAh/g (280 mAh/g based on ZnS mass) to 498 mAh/g (498 mAh/g based on ZnS mass). To understand the physical origin of this enhancement, we conducted electrochemical impedance spectroscopy (EIS) on the half-cells[37,39]. EIS of the as-prepared ZnS nanofibers showed at least one large semicircle that overlapped with the low-frequency diffusion region. After annealing, we observed two changes to the EIS spectrum: a decrease in semicircle radius which reflected a decrease in charge transfer resistance that may partially be attributed to the loss of grain boundaries during annealing[40]. There was also a significant increase in the slope of the low-frequency spectrum, suggesting a more capacitor-like diffusion behavior at lower frequencies, possibly due to an increase in the sodium ion diffusion

coefficient. In addition, the increased ~~This increase could in part be attributed to the increase in particle size. Two reasons were hypothesized for this: (1) as the primary particle size was increased, the amount of particle interfaces/grain boundaries was reduced and electrical conductivity could be increased which would increase active material utilization, (2) increasing~~ particle size after annealing ~~had a simultaneous effect on decreasing the surface area exposed to the electrolyte,~~ led to a decrease in the total particle surface area exposed to the electrolyte, ~~therefore decreasing the solid-electrolyte interface area~~therefore decreasing the SEI surface area. ~~(which also explains why the 1st cycle CE increased from 51% to 69% after annealing as the volume of SEI relative to the volume of accessible active material increases).~~ The SEI is known to be both electrically and ionically insulating, ~~which may further reduce the accessible active material.~~therefore reducing the amount of SEI may have facilitated electron and sodium ion access to the active material. This further explained why the 1st cycle CE increased from 51% to 69% after annealing, as the volume of SEI relative to the volume of accessible active material was increased. A slight increase in average discharge potential from 0.44 V to 0.47 V was also observed. Further increase in reversible capacity to ~~was achieved by carbon-coating, with up to~~ 531 mAh/g was achieved by carbon-coating (603 mAh/g based on ZnS mass, which was roughly the theoretical capacity of 571 mAh/g). The EIS spectrum of carbon-coated ZnS showed at least two smaller semicircles, suggesting further reduced charge transfer resistance at the ZnS, as well as an additional charge transfer process associated with the carbon layer. Carbon is known to undergo electrochemical processes with sodium ion based on a combination of insertion/extraction and pseudocapacitance[41,42]. ~~-~~The average discharge potential decreased to 0.37 V, ~~but~~ while 1st cycle CE remained relatively unchanged at 71% compared to the annealed sample. The gravimetric

and volumetric capacities, initial Coulombic efficiencies, as well as discharge potentials are summarized in Table 3.

~~-~~Galvanostatic cycling was continued for 100 cycles to investigate the effects of post-processing on capacity retention (Figure 4a). The as-prepared nanofibers had a rapid initial drop in capacity, losing almost all capacity by the 10th cycle and retaining only 3% by the 10th cycle. Annealing significantly improved capacity retention. 50% of the 2nd cycle capacity could be retained until the 24th cycle, and after 100 cycles, the material still had 100 mAh/g of capacity. Carbon-coating improved capacity retention even further, retaining 178 mAh/g of capacity after 100 cycles.

Both annealing and carbon-coating significantly improved the electrochemical performance of zinc sulfide nanofibers. The best performing sample was the carbon-coated sample, even when the additional mass of the carbon coating was accounted for.~~.~~

~~-~~We ~~further~~ investigated the stability of the carbon-coated nanofibers using galvanostatic cycling under different discharge ~~charge/discharge~~ rates (Figure 4d). The discharge rate was increased stepwise, from 50 mA/g to 100 mA/g, 200 mA/g, 300 mA/g and up to 400 mA/g. Good rate capability was demonstrated up to 300 mA/g, and a ~~The materials show a good rate capability and capacity retention at a relatively higher current density of 400 mA/g, with a~~ reversible capacity of 252 mAh/g ~~being recovered when the applied current density is switched to 200 mA/g~~could be recovered when the discharge rate was reduced back to 200 mA/g, thus demonstrating reversibility of the material. ~~The~~ CV measurement of the carbon~~-~~-coated nanofiber was taken at a scan rate of 1 mV/s. An irreversible reduction peak at ~0.9 V vs. Na/Na^+ was observed during the first cycle,

which was attributed to the initial formation of the SEI. The cyclic voltammograms stabilized by the 5th cycle, showing a major reversible reduction peak at ~0.5 V and a major oxidation peak at ~0.9 V (Figure 4c).

~~also indicates that 1st irreversible reduction accounts for the initial sodium ion intercalation to the materials and the formation of SEI on the surface of the nanofiber. The following reduction (~0.5 V) and oxidation (~0.9 V) peaks at the 5th cycle match well with these peaks at the 10th cycle, suggesting a good reversibility of the carbon-coated ZnS nanofibers used as sodium ion battery anodes (Figure 4c). We compared~~The ~~the~~ electrochemical performance of ~~this biotemplated material~~biotemplated carbon-coated zinc sulfide nanofibers was compared against other zinc sulfide-based SIB anodes (Table 4). The reversible capacity of this~~of our~~ material was on-par with the highest recorded values (603 mAh/g compared to 610 mAh/g), ~~with higher active material loading (~~even at a higher loading of 80% compared to the more typically reported ~60%~~). and comparatively good initial Coulombic efficiency (71%).~~ The initial capacity of 71% was also comparatively high. In addition, we reported more stable cycling compared to the previous reports (Table 4~~4~~).

~~We further applied post~~Post-mortem XPS and TEM were used to analyze the composition and morphology of the SEI ~~formed on the surface of the~~on carbon-coated ZnS nanofibers at the different stages of the initial cycles (1: first discharge to 0.3 V, 2: first discharge to 0.05 V, 3: first recharge to 3 V and 4: second discharge to 0.05 V) (Figure 5 and Figure S3). TEM image of the ZnS nanofiber showed a thickening of the outermost amorphous layer after the cell was discharged to 0.3 V. This was

Significant SEI formation was observed ~~even~~ when the cell was discharged to 0.3 V, ~~suggesting~~ which suggested that initial~~that the main stage of SEI layer formation due to the~~ electrolyte decomposition and SEI formation had occurred ~~was~~ during the initial sodium ~~intercalation~~ insertion into the nanofiber. ~~TEM image of the ZnS nanofiber shows that the outer most layer was thickened when the cell was discharged to 0.3 V.~~ XPS C1s and O1s high resolution scan at this stage reveals that the interfaces are mostly composed of carbonates, polycarbonate or polyethylene oxides[43,44]. The compositions of the SEI vary upon further discharge and recover a little upon recharge, meanwhile the morphology of the ZnS nanofiber doesn't change. This probably indicates that carbon coating can regulate the SEI formation upon charge and discharge and maintain a thin interface that allow good sodium ion transport through the materials.

Formatted: Font color: Accent 1

Formatted: Indent: First line: 0"

Conclusions

We demonstrated that the M13 bacteriophage ~~can~~ could be used as a biotemplate to synthesize ~~well formed~~ nanofibers of zinc- sulfide~~sulfide, that can be used for sodium ion battery anodes~~, opening up a ~~,~~new approach to synthesizing nanostructured ZnS with highly promising electrochemical performance for SIB anodes. ~~The zinc sulfide~~The biotemplated zinc sulfide nanofibers, after ~~post processing either by pure annealing~~annealing and carbon-coating~~ or molecular templated carbon coating, , showed good electrochemical performance as anode materials for SIBs~~achieved a reversible capacity of 603 mAh/g at 100 mA/g discharge rate even at a high overall zinc sulfide loading of 70%. Initial Coulombic efficiency was as high as 71%, and the material could be cycled for at least 100 cycles. However, at the benchtop scale, the use of

biotemplating did increase the cost of zinc sulfide synthesis significantly (additional $50 per g of ZnS), and future work should address cost reduction.

~~. We found that both annealing and carbon-coating of the zinc sulfide nanofibers can enhance initial coulombic efficiency by increasing particle size and reducing active contact between the zinc sulfide and the electrolyte, therefore, increase the capacity and cycling stability of the sodium ion batteries. Biotemplated zinc sulfide nanofibers when coated with a <2 nm carbon layer could deliver a reversible capacity of 603 mAh/g at 100 mA/g discharge rate, even with a high overall zinc sulfide loading of 70%. Initial Coulombic efficiency was as high as 71%, and the cell could be cycled for at least 100 cycles.~~

Experimental

Synthesis of zinc sulfide nanofibers

In a typical synthesis, 200 mL of 6.4×10^{11} pfu/mL M13 bacteriophage (EEAE clone) was preheated at 95 °C for 1 hour. 1 mL of 1 M zinc acetate (Alfa Aesar, 97%) was added, followed by 6 mL 0.5 M thioacetamide (Sigma-Aldrich, 99%) under gentle shaking. The thioacetamide did not completely dissolve in water, and was therefore filtered over a 0.2 μm filter membrane to remove the small amount of undissolved chemical. After initial mixing, the reaction was allowed to proceed for 3 hours at 95 °C with no further mechanical agitation. The as-prepared nanofibers were collected by centrifugation at 3500 rpm, and then washed 2 times with water. The materials were then lyophilized to retain as much surface area as possible (sample M13-ZnS). Annealing of the nanofibers was done at 600 annealed at 600 °C for 1 hour under flowing Argon using 10 °C/min heating rate (sample M13-ZnS600).

Carbon-coating of zinc sulfide nanofibers

Resin-coating was typically done in a 50 mL reaction. 1.5 mL 1.67 M resorcinol, 1.5 mL 10 vol. % formaldehyde and 450 µL of 1 vol. % ethylenediamine were added to a suspension of zinc sulfide nanofibers (at a concentration of 2×10^{13} mL^{-1} based on the number of virus particles assuming each virus particle corresponds to a single nanofiber). The reaction mixture was heated to 80 °C and allowed to react for at least 12 hours with no mechanical agitation. Resin-coated nanofibers were collected by centrifugation, washed and air dried. Carbonization was carried out in flowing Argon at 600 °C for 1 hour using 10 °C/min heating rate (sample M13-ZnS600C).

Material characterization

The morphology and lattice spacing of the nanofibers was viewed using transmission electron microscopy at 200 kV (TEM, JEOL JEM-2010). Electron diffraction (ED) patterns were obtained using the FEI Tecnai G2 Sprint TWIN at 120 kV. Elemental binding states were probed using X-ray photoelectron spectroscopy (XPS, Thermo Scientific K-Alpha). Crystal structure and crystal size were investigated using X-ray diffractometry (XRD, Panalytical X'Pert Pro Multipurpose Diffractometer) in the Bragg-Brentano geometry between 10° and 80° 2θ using a copper source. Surface area was measured using Brunauer–Emmett–Teller (BET, Micromeritics ASAP 2020). Carbon content was estimated using thermogravimetric analysis (TGA, TA Instruments Discovery) in air using a linear ramp mode (10 °C/min) from 40 °C to 800 °C.

Electrochemical Measurements

2032 coin-type cells were assembled using sodium metal foil (Sigma-Aldrich) as the anode electrode, glass fiber membranes (Sigma-Aldrich) as the separator, and a cathode composed of a mixture of 80% zinc sulfide nanofibers, 10% Super-P Li carbon black (TIMCAL) and 10% poly(vinylidene difluoride) (Sigma-Aldrich), and an electrolyte of 80 μL of 1 M sodium perchlorate ($NaClO_4$) in ethylene carbonate and propylene carbonate (v/v = 1:1) with 5 wt. % fluoroethylene carbonate (Sigma-Aldrich) as the additive. Cell assembly was carried out in an argon-filled glovebox (MBraun Labmaster). The room-temperature cycling characteristics of the cells were evaluated under galvanostatic conditions using Land battery testers, and electrochemical processes in the cells were studied by cyclic voltammetry and impedance using the Biologic VMP-3 Potentiostat.

FIGURES

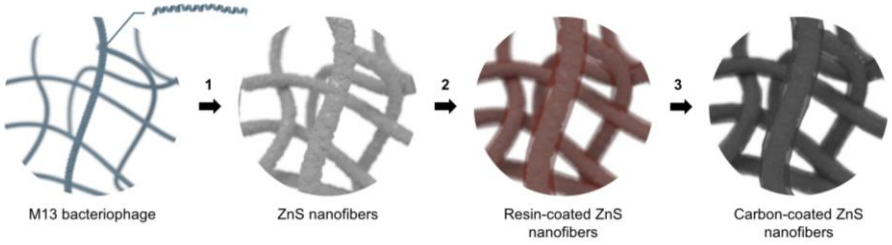

Figure 1. Schematic showing the ~~overall~~ complete process for preparing carbon-coated zinc sulfide nanofibers using biotemplating. Step (1) is a mild, aqueous reaction, where 5 mM zinc acetate ~~were~~ was reacted with 15 mM thioacetamide at 95 °C for 2~3 hours to form zinc sulfide nanofibers. Step (2) is ~~the~~ resin-coating ~~step~~, where the as-prepared zinc sulfide nanofibers were

Formatted: Normal, Space After: 0 pt

incubated in a solution of resorcinol, formaldehyde and ethylenediamine at 80 °C overnight to form a thin phenolic resin coating. Step (3) is the final carbonization ~~step~~, where the resin-coated nanofibers were heated in flowing Argon at 600 °C for 1 hour (~~, with a~~ 10 °C/min ramp rate with furnace cooling) to achieve the final carbon-coated zinc sulfide nanofibers.

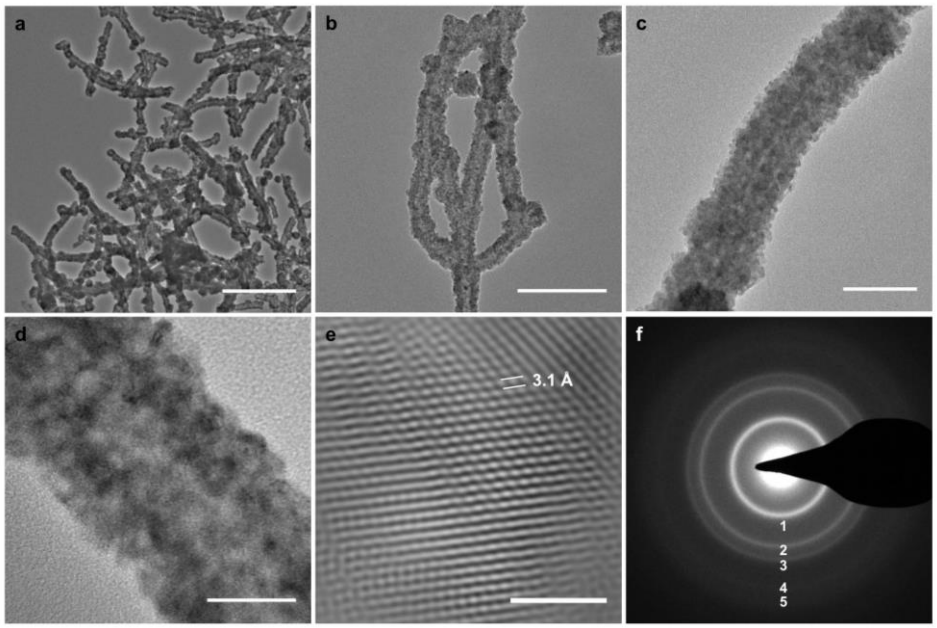

Figure 2. Morphological and structural characterization of biotemplated zinc sulfide nanofibers ~~prepared by biotemplating~~. ~~Images~~ Figures (a)-(d) are TEM micrographs at various magnifications. Most nanofibers ~~had~~ contained a hollow interior ~~due to the~~as a result of the precipitation-aggregation mechanism. ~~responsible for their synthesis.~~ The low-contrast virus template core can clearly be seen in image (c). ~~Image~~ Figure (e) is the high-~~-~~resolution lattice image with the (111) interplanar spacing of 3.1 Å labeled. The electron diffraction pattern is shown in

Formatted: Normal
Formatted: Font: Times

image (f), and the . The diffraction rings corresponding to planes 1 (111), 2 (220), 3 (311), 4 (331) and 5 (422) are clearly visiblelabeled. Scale bars: (a) 500 nm, (b) 200 nm, (c) 50 nm, (d) 20 nm and (e) 10 nm.

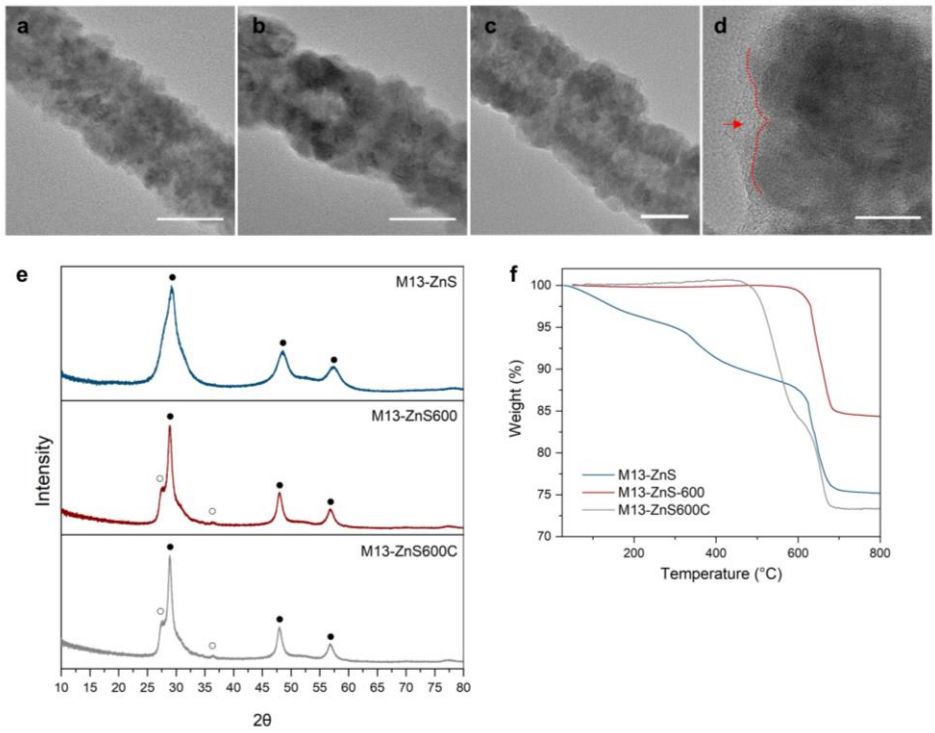

Figure 3. Morphological and structural comparisons between as-prepared zinc sulfide nanofibers (M13-ZnS), nanofibers after annealing at 600 °C (M13-ZnS600) and after carbon-coating at 600 °C (M13-ZnS600C). Figures (a)-(cd) are TEM micrographs showing the increase in primary particle size after annealing and carbon-coating; the morphology of the nanofibers remained unchangedstructural changes due to annealing and carbon coatin.g. Figure (d) is a higher

Formatted: Normal
Formatted: Font: Times

resolution image of sample M13-ZnS600C, a thin carbon coating is resolved and label (arrow and dotted line). ~~Image (a) shows the as-prepared nanofiber, with small primary particle size. Image (b) shows the nanofiber after annealing at 600 °C for 1 hour showing a slight increase in primary particle size. Image (c) and (d) are images of the nanofiber after carbon-coating. Structurally, this sample was very similar to the annealed nanofiber. However, under higher resolution, a very thin layer of amorphous carbon coating 1.3~1.9 nm in thickness could be resolved.~~ Scale bars: (a) 30 nm, (b) 30 nm, (c) 30 nm and (d) 15 nm. Figure (e) shows the XRD diffractograms- of the three samples~~of Figure (f) shows the XRD diffractograms~~. Peaks corresponding to cubic-phase β-ZnS are labelled with filled circles and peaks corresponding to hexagonal-phase ZnS are labeled with unfilled circles✦. Figure (f) shows the TGA thermograms ~~with a linear~~taken using a linear ramp from 20 °C to 800 °C at 10 °C/min in air. ~~The four different regions of thermal decompositions are labelled 1-4.~~

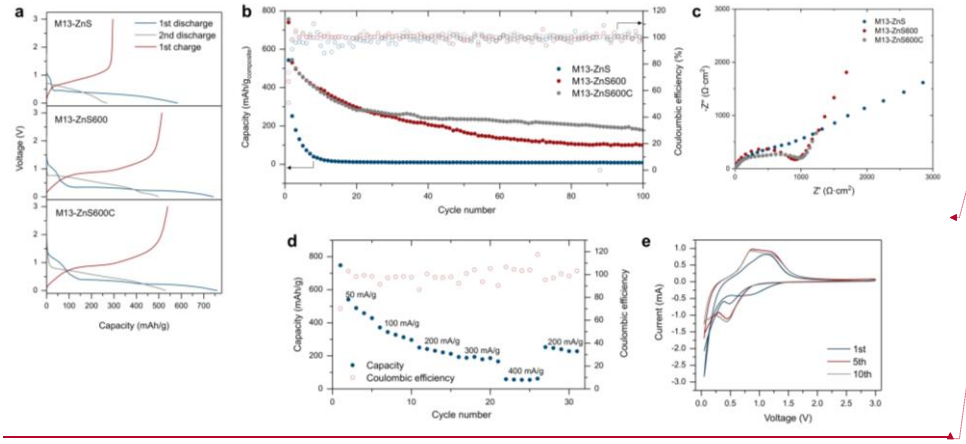

Formatted: Normal

Formatted: Font: Times

Figure 4. Electrochemical performance of biotemplated zinc sulfide nanofibers in ~~in~~ SIBs against a sodium metal counter-electrode. Figure (a) shows the voltage profile for the 1st and 2nd cycle discharge, as well as the 1st cycle charge at 50 mA/g. Figure (b~~a~~) shows the cycling stability of the different types of nanofibers at 50 mA/g charge and discharge rates between 0 and 3 V. The capacity is normalized against total composite mass. Figure (c) shows the EIS spectra of the different samples. ~~Figure (b) shows the voltage profile for the 1st and 2nd cycle discharge, as well as the 1st cycle charge at 50 mA/g.~~ Figure (d) shows the galvanostatic cycling performance of the carbon-coated nanofiber (M13-ZnS600C) at 50 mA/g, 100 mA/g, 200 mA/g, 300 mA/g and 400 mA/g charge and discharge rates. Figure (e) ~~(c)~~ is the cyclic ~~voltammetry~~ voltammogram of ~~carbon-coated sample~~sample M13-ZnS600C ~~up to the 10th cycle~~ at a sweep rate of 0.1 mV/s for the 1st, 5th and 10th cycles. ~~Figure (d) shows the capacity retention of the carbon-coated nanofibers (M13-ZnS600C) under different cycling rates.~~

Formatted: Superscript

Formatted: Superscript

Formatted: Superscript

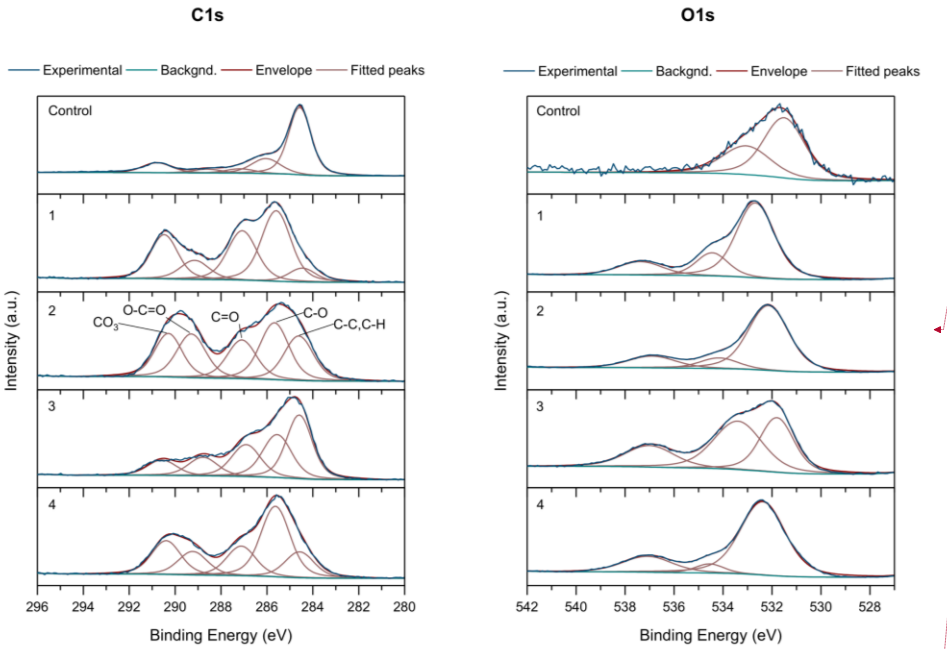

Figure 5. XPS (C1s and O1s) characterization of the solid-electrolyte interface on sample M13-ZnS600C~~the ZnS nanofibers~~ at different levels of discharge and charge. ~~Point 1~~The sample was discharged to 0.3 V (point 1), ~~point 2 was~~then discharged further to 0.05 V (point 2), ~~point 3 was~~ recharged to 3 V (point 3) and ~~point 4 was discharged again to 0.05 V.~~discharged again back to 0.05 V (point 4).

TABLES

Table 1. Prices of some transition metals used for sulfide-type anodes in SIBs.~~.~~

Metal	$ per lb

Formatted: Normal

Formatted: Font: Times

Cu	2.16
Ni	4.22
Zn	0.92
Mo	6.58
W (WO_3)	8.11
Sn	7.45

Table 2. Physical properties and composition of biotemplated zinc sulfide nanofibers.

	Surface area (m^2/g)	Crystallite size (nm)	Wt. % ZnS
M13-ZnS	26.1	4.4	90
M13-ZnS600	18.9	9.6	101
M13-ZnS600C	74.2	9.5	88

Table 3. Summary of galvanostatic cycling performance at 50 mA/g over the first two cycles for different biotemplated zinc sulfide nanofibers.

	Reversible gravimetric capacity (mAh/g)	Reversible volumetric capacity (mAh/cm^3)	1^{st} cycle CE (%)	Average discharge voltage (V)
M13-ZnS	252	92	51	0.44
M13-ZnS600	498	183	69	0.47
M13-ZnS600C	531	195	71	0.37

Table 44. Comparison of the electrochemical performance of biotemplated ZnS against other ZnS-based anodes for SIBs reported in the literature.

Materials	Initial C.E.	ZnS loading	Reversible Capacity (mAh/g_{ZnS})	Number of cycles	Current density	Reference
ZnS-RGO	57%	40%	610	50	100 mA/g	45
ZnS@d-PPy	65.40%	63%	475	30	100 mA/g	46
ZnS/NSC	65.90%	59%	561.2	100	100 mA/g	15
ZnS nanosphere	77.10%	N/A	610	30	80mA/g	47
ZnS nanofiber	71%	70%	603	100	100 mA/g	This work

Formatted Table
Field Code Changed
Formatted: Not Superscript/ Subscript
Field Code Changed
Formatted: Not Superscript/ Subscript
Field Code Changed
Formatted: Not Superscript/ Subscript
Field Code Changed
Formatted: Not Superscript/ Subscript

ASSOCIATED CONTENT

Supporting Information.

Supplementary Figure S1: TEM images of ZnS nanofibers/nanoparticles synthesized using the wild-type M13 bacteriophage template.

Formatted: Indent: First line: 0"

Supplementary Figure S2: High resolution XPS spectrum of Zn2p, showing a slight shift in peak position after carbon-coating.

Supplementary Figure S3: TEM images showing the morphological stability of ZnS nanofibers at different levels of discharge/recharge. The sample was discharged to 0.3 V (point 1), then discharged further to 0.05 V (point 2), recharged to 3 V (point 3) and discharged again back to 0.05 V (point 4).

~~Point 1 was discharged to 0.3 V, point 2 was discharged to 0.05 V, point 3 was recharged to 3 V and point 4 was discharged again to 0.05 V.~~

AUTHOR INFORMATION

Corresponding Author

~~*~~Angela M. Belcher~~.~~ Email: belcher@mit.edu

Author Contributions

All authors conceived the work. G.Z. and S.W. conducted the experiments. A.M.B. supervised the work. The manuscript was written through contributions of all authors. All authors have given approval to the final version of the manuscript.

Funding Sources

This work was funded by the U.S. Defense Advanced Research Projects Agency's Living Foundries program award HR0011-15-C-0084 and the Army Research Office Institute of Collaborative Biotechnologies (ICB) Grant #017251-022.

ACKNOWLEDGMENT

(Word Style "TD_Acknowledgments"). Generally the last paragraph of the paper is the place to acknowledge people, organizations, and financing (you may state grant numbers and sponsors here). Follow the journal's guidelines on what to include in the Acknowledgments section.

ABBREVIATIONS

SIB, sodium-ion battery; CE, Coulombic efficiency.

REFERENCES

(1) Sotiropoulou, S.; Sierra-Sastre, Y.; Mark, S. S.; Batt, C. A. Biotemplated Nanostructured Materials. *Chem. Mater.* **2008**, *20*, 821–834.

(2) Zhou, H.; Fan, T.; Zhang, D. Biotemplated Materials for Sustainable Energy and Environment: Current Status and Challenges. *ChemSusChem* **2011**, *4*, 1344–1387.

(3) Mao, C. Virus-Based Toolkit for the Directed Synthesis of Magnetic and Semiconducting Nanowires. *Science (80-.).* **2004**, *303*, 213–217.

(4) Nam, K. T. Virus-Enabled Synthesis and Assembly of Nanowires for Lithium Ion Battery Electrodes. *Science (80-.).* **2006**, *312*, 885–888.

(5) Hess, G. T.; Cragnolini, J. J.; Popp, M. W.; Allen, M. A.; Dougan, S. K.; Spooner, E.; Ploegh, H. L.; Belcher, A. M.; Guimaraes, C. P. M13 Bacteriophage Display Framework That Allows Sortase-Mediated Modification of Surface-Accessible Phage Proteins. *Bioconjug. Chem.* **2012**, *23*, 1478–1487.

(6) Verheust, C.; Pauwels, K.; Mahillon, J.; Helinski, D. R.; Herman, P. Contained Use of Bacteriophages: Risk Assessment and Biosafety Recommendations. *Appl. Biosaf.* **2010**, *15*, 32–44.

(7) Manivannan, S.; Kang, I.; Seo, Y.; Jin, H. E.; Lee, S. W.; Kim, K. M13 Virus-Incorporated Biotemplates on Electrode Surfaces to Nucleate Metal Nanostructures by Electrodeposition. *ACS Appl. Mater. Interfaces* **2017**, *9*, 32965–32976.

(8) Emami, F. S.; Puddu, V.; Berry, R. J.; Varshney, V.; Patwardhan, S. V.; Perry, C. C.; Heinz, H. Prediction of Specific Biomolecule Adsorption on Silica Surfaces as a Function of PH and Particle Size. *Chem. Mater.* **2014**, *26*, 5725–5734.

(9) Nam, Y. S.; Magyar, A. P.; Lee, D.; Kim, J.-W.; Yun, D. S.; Park, H.; Pollom, T. S.; Weitz, D. a; Belcher, A. M. Biologically Templated Photocatalytic Nanostructures for Sustained Light-Driven Water Oxidation. *Nat. Nanotechnol.* **2010**, *5*, 340–344.

(10) Scholz, S. M.; Vacassy, R.; Lemaire, L.; Dutta, J.; Hofmann, H. Nanoporous Aggregates of ZnS Nanocrystallites. *Appl. Organomet. Chem.* **1998**, *12*, 327–335.

(11) Zhao, Q.; Xie, Y.; Zhang, Z.; Bai, X. Size-Selective Synthesis of Zinc Sulfide Hierarchical Structures and Their Photocatalytic Activity. *Cryst. Growth Des.* **2007**, *7*, 153–158.

(12) Yang, Y.; Zhang, W. Preparation and Photoluminescence of Zinc Sulfide Nanowires. *Mater. Lett.* **2004**, *58*, 3836–3838.

(13) Lai, C.-H.; Lu, M.-Y.; Chen, L.-J. Metal Sulfide Nanostructures: Synthesis, Properties and Applications in Energy Conversion and Storage. *J. Mater. Chem.* **2012**, *22*, 19–30.

(14) Li, J.; Fu, Y.; Shi, X.; Xu, Z.; Zhang, Z. Urchinlike ZnS Microspheres Decorated with Nitrogen-Doped Carbon: A Superior Anode Material for Lithium and Sodium Storage. *Chem. - A Eur. J.* **2017**, *23*, 157–166.

(15) Jing, M.; Chen, Z.; Li, Z.; Li, F.; Chen, M.; Zhou, M.; He, B.; Chen, L.; Hou, Z.; Chen, X. Facile Synthesis of ZnS/N,S Co-Doped Carbon Composite from Zinc Metal Complex for High-Performance Sodium-Ion Batteries. *ACS Appl. Mater. Interfaces* **2018**, *10*, 704–712.

(16) Choudhury, S.; Wei, S.; Ozhabes, Y.; Gunceler, D.; Zachman, M. J.; Tu, Z.; Shin, J. H.; Nath, P.; Agrawal, A.; Kourkoutis, L. F.; et al. Designing Solid-Liquid Interphases for Sodium Batteries. *Nat. Commun.* **2017**, *8*, 1–10.

(17) Lee, M.; Hong, J.; Lopez, J.; Sun, Y.; Feng, D.; Lim, K.; Chueh, W. C.; Toney, M. F.; Cui, Y.; Bao, Z. High-Performance Sodium-Organic Battery by Realizing Four-Sodium Storage in Disodium Rhodizonate. *Nat. Energy* **2017**, *2*, 861–868.

(18) Zhu, Y.; Han, X.; Xu, Y.; Liu, Y.; Zheng, S.; Xu, K.; Hu, L.; Wang, C. Electrospun Sb/C Fibers for a Stable and Fast Sodium-Ion Battery Anode. *ACS Nano* **2013**, *7*, 6378–6386.

(19) Wei, S.; Choudhury, S.; Xu, J.; Nath, P.; Tu, Z.; Archer, L. A. Highly Stable Sodium Batteries Enabled by Functional Ionic Polymer Membranes. *Adv. Mater.* **2017**, *29*, 1605512.

(20) Wu, D.; Li, X.; Xu, B.; Twu, N.; Liu, L.; Ceder, G. $NaTiO_2$: A Layered Anode Material for Sodium-Ion Batteries. *Energy Environ. Sci.* **2015**, *8*, 195–202.

(21) Li, F.; Zhou, Z. Micro/Nanostructured Materials for Sodium Ion Batteries and Capacitors. *Small* **2018**, *14*, 1–25.

(22) Yabuuchi, N.; Kubota, K.; Dahbi, M.; Komaba, S. Research Development on Sodium-Ion Batteries. *Chem. Rev.* **2014**, *114*, 11636–11682.

(23) Liu, L.; Li, X.; Bo, S. H.; Wang, Y.; Chen, H.; Twu, N.; Wu, D.; Ceder, G. High-Performance P2-Type Na2/3(Mn1/2Fe1/4Co1/4)O2 Cathode Material with Superior Rate Capability for Na-Ion Batteries. *Adv. Energy Mater.* **2015**, *5*, 1–5.

(24) Wei, S.; Cheng, Z.; Nath, P.; Tikekar, M. D.; Li, G.; Archer, L. A. Stabilizing

Electrochemical Interfaces in Viscoelastic Liquid Electrolytes. *Sci. Adv.* **2018**, *4*, 1–9.

(25) Seh, Z. W.; Sun, J.; Sun, Y.; Cui, Y. A Highly Reversible Room-Temperature Sodium Metal Anode. *ACS Cent. Sci.* **2015**, *1*, 449–455.

(26) Bai, P.; He, Y.; Xiong, P.; Zhao, X.; Xu, K.; Xu, Y. Long Cycle Life and High Rate Sodium-Ion Chemistry for Hard Carbon Anodes. *Energy Storage Mater.* **2018**, *13*, 274–282.

(27) Xiao, Y.; Lee, S. H.; Sun, Y. K. The Application of Metal Sulfides in Sodium Ion Batteries. *Adv. Energy Mater.* **2017**, *7*, 1601329.

(28) Ge, P.; Zhang, C.; Hou, H.; Wu, B.; Zhou, L.; Li, S.; Wu, T.; Hu, J.; Mai, L.; Ji, X. Anions Induced Evolution of Co3X4(X = O, S, Se) as Sodium-Ion Anodes: The Influences of Electronic Structure, Morphology, Electrochemical Property. *Nano Energy* **2018**, *48*, 617–629.

(29) Chen, Y. M.; Yu, X. Y.; Li, Z.; Paik, U.; Lou, X. W. Hierarchical MoS2 Tubular Structures Internally Wired by Carbon Nanotubes as a Highly Stable Anode Material for Lithium-Ion Batteries. *Sci. Adv.* **2016**, *2*, e1600021–e1600021.

(30) Liu, Y.; Yu, X. Y.; Fang, Y.; Zhu, X.; Bao, J.; Zhou, X.; Lou, X. W. (David). Confining SnS2Ultrathin Nanosheets in Hollow Carbon Nanostructures for Efficient Capacitive Sodium Storage. *Joule* **2018**, *2*, 725–735.

(31) Sheng, J.; Yang, L.; Zhu, Y. E.; Li, F.; Zhang, Y.; Zhou, Z. Oriented SnS Nanoflakes Bound on S-Doped N-Rich Carbon Nanosheets with a Rapid Pseudocapacitive Response as High-Rate Anodes for Sodium-Ion Batteries. *J. Mater. Chem. A* **2017**, *5*, 19745–19751.

(32) Grau, J.; Akinc, M. Synthesis of Nickel Sulfide by Homogeneous Precipitation from Acidic Solutions of Thioacetamide.Pdf. *Journal of the American Ceramic Society*. 1996, pp 1073–1082.

(33) Arul Dhas, N.; Zaban, a; Gedanken, a. Surface Synthesis of Zinc Sulfide Nanoparticles on Silica Microspheres: Sonochemical Preparation, Characterization and Optical Properties. *Chem. Mater.* **1999**, *11*, 806.

(34) Velikov, K. P.; Van Blaaderen, A. Synthesis and Characterization of Monodisperse Core-Shell Colloidal Spheres of Zinc Sulfide and Silica. *Langmuir* **2001**, *17*, 4779–4786.

(35) De Mello Donegá, C.; Liljeroth, P.; Vanmaekelbergh, D. Physicochemical Evaluation of the Hot-Injection Method, a Synthesis Route for Monodisperse Nanocrystals. *Small* **2005**, *1*, 1152–1162.

(36) Haile, S. M.; Johnson, D. W.; Wiseman, G. H.; Bowen, H. K. Aqueous Precipitation of Spherical Zinc Oxide Powders for Varistor Applications. *J. Am. Ceram. Soc.* **1989**, *72*, 2004–2008.

(37) Ge, P.; Hou, H.; Ji, X.; Huang, Z.; Li, S.; Huang, L. Enhanced Stability of Sodium Storage Exhibited by Carbon Coated Sb2S3hollow Spheres. *Mater. Chem. Phys.* **2018**, *203*, 185–192.

(38) Kole, A. K.; Kumbhakar, P. Cubic-to-Hexagonal Phase Transition and Optical Properties of Chemically Synthesized ZnS Nanocrystals. *Results Phys.* **2012**, *2*, 150–155.

(39) Ruffo, R.; Sae Hong, S.; Chan, C. K.; Huggins, R. A.; Cui, Y. Impedance Analysis of Silicon

Nanowire Lithium Ion Battery Anodes. **2009**, 11390–11398.

(40) Amin, R.; Maier, J. Effect of Annealing on Transport Properties of LiFePO4: Towards a Defect Chemical Model. *Solid State Ionics* **2008**, *178*, 1831–1836.

(41) Ge, P.; Hou, H.; Cao, X.; Li, S.; Zhao, G.; Guo, T.; Wang, C.; Ji, X. Multidimensional Evolution of Carbon Structures Underpinned by Temperature-Induced Intermediate of Chloride for Sodium-Ion Batteries. *Adv. Sci.* **2018**, *5*.

(42) Hou, H.; Banks, C. E.; Jing, M.; Zhang, Y.; Ji, X. Carbon Quantum Dots and Their Derivative 3D Porous Carbon Frameworks for Sodium-Ion Batteries with Ultralong Cycle Life. *Adv. Mater.* **2015**, *27*, 7861–7866.

(43) Zheng, J.; Engelhard, M. H.; Mei, D.; Jiao, S.; Polzin, B. J.; Zhang, J. G.; Xu, W. Electrolyte Additive Enabled Fast Charging and Stable Cycling Lithium Metal Batteries. *Nat. Energy* **2017**, *2*, 1–8.

(44) Muñoz-Márquez, M. A.; Zarrabeitia, M.; Castillo-Martínez, E.; Eguía-Barrio, A.; Rojo, T.; Casas-Cabanas, M. Composition and Evolution of the Solid-Electrolyte Interphase in Na2Ti3O7 Electrodes for Na-Ion Batteries: XPS and Auger Parameter Analysis. *ACS Appl. Mater. Interfaces* **2015**, *7*, 7801–7808.

(45) Qin, W.; Li, D.; Zhang, X.; Yan, D.; Hu, B.; Pan, L. ZnS Nanoparticles Embedded in Reduced Graphene Oxide as High Performance Anode Material of Sodium-Ion Batteries. *Electrochim. Acta* **2016**, *191*, 435–443.

(46) Hou, T.; Tang, G.; Sun, X.; Cai, S.; Zheng, C.; Hu, W. Perchlorate Ion Doped Polypyrrole

Coated ZnS Sphere Composites as a Sodium-Ion Battery Anode with Superior Rate Capability Enhanced by Pseudocapacitance. *RSC Adv.* **2017**, *7*, 43636–43641.

(47) Su, D.; Kretschmer, K.; Wang, G. Improved Electrochemical Performance of Na-Ion Batteries in Ether-Based Electrolytes: A Case Study of ZnS Nanospheres. *Adv. Energy Mater*. **2016**, *6*, 1–13.